

Depth-dependent magnetism in epitaxial MnSb thin films: effects of surface passivation and cleaning

This article has been downloaded from IOPscience. Please scroll down to see the full text article.

2012 J. Phys.: Condens. Matter 24 146002

(<http://iopscience.iop.org/0953-8984/24/14/146002>)

View [the table of contents for this issue](#), or go to the [journal homepage](#) for more

Download details:

IP Address: 137.205.50.42

The article was downloaded on 18/04/2013 at 21:18

Please note that [terms and conditions apply](#).

Depth-dependent magnetism in epitaxial MnSb thin films: effects of surface passivation and cleaning

J D Aldous¹, C W Burrows¹, I Maskery¹, M S Brewer¹, T P A Hase¹,
J A Duffy¹, M R Lees¹, C Sánchez-Hanke², T Decoster³, W Theis³,
A Quesada⁴, A K Schmid⁴ and G R Bell¹

¹ Department of Physics, University of Warwick, Coventry, CV4 7AL, UK

² National Synchrotron Light Source, Brookhaven National Laboratory, Upton, NY 11973-5000, USA

³ Department of Physics and Astronomy, University of Birmingham, Birmingham B15 2TT, UK

⁴ National Center for Electron Microscopy, Lawrence Berkeley National Laboratory, Berkeley, CA 94720-8250, USA

E-mail: gavin.bell@physics.org

Received 1 December 2011, in final form 24 February 2012

Published 15 March 2012

Online at stacks.iop.org/JPhysCM/24/146002

Abstract

Depth-dependent magnetism in MnSb(0001) epitaxial films has been studied by combining experimental methods with different surface specificities: polarized neutron reflectivity, x-ray magnetic circular dichroism (XMCD), x-ray resonant magnetic scattering and spin-polarized low energy electron microscopy (SPLEEM). A native oxide ~ 4.5 nm thick covers air-exposed samples which increases the film's coercivity. HCl etching efficiently removes this oxide and *in situ* surface treatment of etched samples enables surface magnetic contrast to be observed in SPLEEM. A thin Sb capping layer prevents oxidation and preserves ferromagnetism throughout the MnSb film. The interpretation of Mn L_{3,2} edge XMCD data is discussed.

(Some figures may appear in colour only in the online journal)

1. Introduction

Magnetic and semiconducting materials in combination have a huge range of potential applications, from spintronic devices [1, 2] to optical isolators [3, 4]. Epitaxial compatibility between the materials is advantageous [5] and transition metal pnictides such as MnSb combine well with III–V semiconductors using molecular beam epitaxy (MBE) [6, 7]. Both for artificial multi-layered magnetic structures and naturally occurring 'layers' such as free surfaces, one often wishes to measure the magnetic behaviour with both elemental and depth specificity. To give recent examples, magnetite (001) surfaces terminated with a monolayer of H retain their bulk-like spin polarization (SP) far more readily than the unpassivated surface [8], while the Co₂MnSi–MgO interface could be rendered free of minority spin interface states by the insertion of an atomic layer of Al in a particular layer ordering [9]. Such effects can

only be studied in isolation by experimental techniques with appropriate depth sensitivity or elemental specificity.

Here we report a study of MBE-grown MnSb(0001) surfaces with and without passivation or cleaning. We combine polarized neutron reflectivity (PNR), spin-polarized low energy electron microscopy (SPLEEM), x-ray magnetic circular dichroism (XMCD) by total electron yield (TEY) and x-ray resonant magnetic scattering (XRMS). These methods reveal the magnetic behaviour with differing depth sensitivity and as a function of surface termination. In PNR, reflectivity curves are fitted with magnetic and structural layer models. By contrast, the surface specificities of SPLEEM and TEY XMCD are defined by the inelastic mean free path (IMFP) of the reflected electrons or photoelectrons respectively [10], typically (0.5–5) nm. In XRMS, reflected photons of different polarizations provide a magnetic signal whose depth sensitivity is more complicated, but when the photon energy is a little below an absorption resonance one

expects to probe the whole of a ≤ 100 nm thick film. These techniques are therefore highly complementary for studies of thin film magnetism, offering insight into the roles of the surface and the interfaces.

MnSb is ferromagnetic (FM) with a Curie temperature T_C of 587 K. Half-metallic pnictides are especially promising since their SP at the Fermi energy may approach 100% [11–13]. While understanding the temperature dependence of their SP remains crucial to exploiting these materials in room-temperature devices [14], it is known that the surfaces [15] and interfaces [16, 17] of half-metals may fail to show high SP even at cryogenic temperatures due to localized minority spin states. A severe problem in understanding these effects has been disentangling the fundamental properties from the role of defects, disorder and magnetic inhomogeneity [18]. While excellent single crystal surfaces can be prepared by MBE, the native oxides are difficult to remove without affecting the stoichiometry [19], morphology [20] and magnetization [21]. We examine here the effects of simple passivation or chemical etching on the near-surface magnetism in MnSb(0001) at room temperature.

2. Experimental details

MnSb(0001) films of varying thickness (50 nm to 1 μm) were grown on GaAs(111)B substrates using MBE [6]. Sb-capped samples were prepared by cooling to 520 K from the growth temperature of 690 K before exposing to a 2×10^{-4} Pa beam equivalent pressure of Sb_4 for 2 min. All samples were removed from the MBE chamber without special precautions and were typically exposed to ambient air for several weeks. Electron and x-ray diffraction confirmed the single crystal epitaxy of the films, with MnSb [0001] parallel to GaAs [111] and MnSb [2 $\bar{1}$ 10] parallel to GaAs [1 $\bar{1}$ 0]. The Sb caps were partly crystalline and epitaxial, and typically several nm thick. Volume-averaged magnetic characteristics were measured by conventional vibrating sample magnetometry (VSM) and superconducting quantum interference device (SQUID) magnetometry. The effects on the sample surface morphology of the different surface preparation methods were also examined by atomic force microscopy (AFM), using an Asylum Research MFP-3D microscope operating in tapping mode. Root-mean-square (RMS) surface roughness values are given based on 5 μm topographs.

The PNR measurements were made on the ADAM beam line at the Institut Laue-Langevin. The specular reflectivity was measured in ambient air at room temperature for several untreated MnSb epilayers of known thicknesses (around 200 nm). The neutron beam was aligned close to a MnSb [1 $\bar{1}$ 00] direction. The neutron wavelength was 4.4 Å and measurements were made at both saturation (1500 Oe) and remanence. Polarization analysis was performed on the reflected beam, yielding ‘uu’ and ‘dd’ channels, where the incident neutron spin was unchanged, as well as the spin-flip channel (not shown). The experiments were restricted to native oxide-covered samples since a vacuum environment was not available.

X-ray experiments were performed at beamline X13A of the National Synchrotron Light Source [22] (NSLS) which reverses the helicity of the 70% circularly polarized x-ray beam at 22 Hz. The sample is held in vacuum and a magnetic field of up to 0.2 T can be applied by an electromagnet, in-plane parallel to the x-ray beam. Pairs of x-ray absorption spectra (XAS) were obtained at room temperature (RT) at $H = \pm 0.2$ T, with each pair averaged to remove experimental artefacts. These were measured by both TEY and reflectivity simultaneously (*no* change of sample conditions), with XMCD and XRMS derived from these spectra respectively. Photons were incident at between 8° and 30° to the surface plane. Uncapped MnSb epilayers were measured prior to and after a 40 s etch in 10 M HCl solution [19]. Data for Sb-capped samples were obtained without further post-growth treatment.

The SPLEEM measurements were performed at the National Center for Electron Microscopy using a dedicated microscope [23] with ~ 10 nm lateral spatial resolution and fully adjustable SP vector (SP 30%) operating in ultra-high vacuum (UHV). Experiments were performed on 10 s HCl-etched samples which were degassed at 400 K for several hours then Ar ion sputtered for ≤ 5 min (energy ≤ 2 keV, beam current ≤ 10 μA) before introduction to UHV. AC demagnetization could be performed with a 50 Hz alternating in-plane field. Samples were annealed to increasing temperatures during LEEM imaging in UHV. Since the temperature was measured by a thermocouple in contact with a Mo sample clamp rather than the sample itself, there is significant systematic uncertainty (± 50 K) in the absolute surface temperature. The low energy electron diffraction (LEED) pattern was also checked after different surface treatments.

3. Results and discussion

We first discuss the surface morphology of the films as a function of surface preparation. After storage in ambient air for several weeks, the uncapped MnSb(0001) epilayers are oxidized [19] and covered in organic surface contamination, producing cloudy-looking AFM topographs with sub-micron sized clusters as shown in figure 1(a). The RMS roughness of such samples is between 0.9 and 1.90 nm. The contamination is readily removed by ultrasonic cleaning in acetone, which reveals very flat (RMS roughness 0.5 nm) epilayer surfaces with some sub-micron sized pits and mesas (figure 1(b)). The RMS roughness increases with HCl etching, from around 2 nm after a 10 s etch to 10 nm for a 40 s etch. The morphology is similar to the sonicated as-grown samples although some micron-scale circular etch features can be seen along with the pits and mesas (figure 1(c)). The roughness of the Sb-capped samples varies from 0.75 to 2.1 nm depending on the total Sb exposure and substrate temperature. The morphology comprises quite uniform and partly merged sub-micron sized Sb islands (figure 1(d)).

In figures 2 and 3 we show typical results for MnSb epilayers from VSM and SQUID magnetometry respectively. The expected FM behaviour appears in all the films studied.

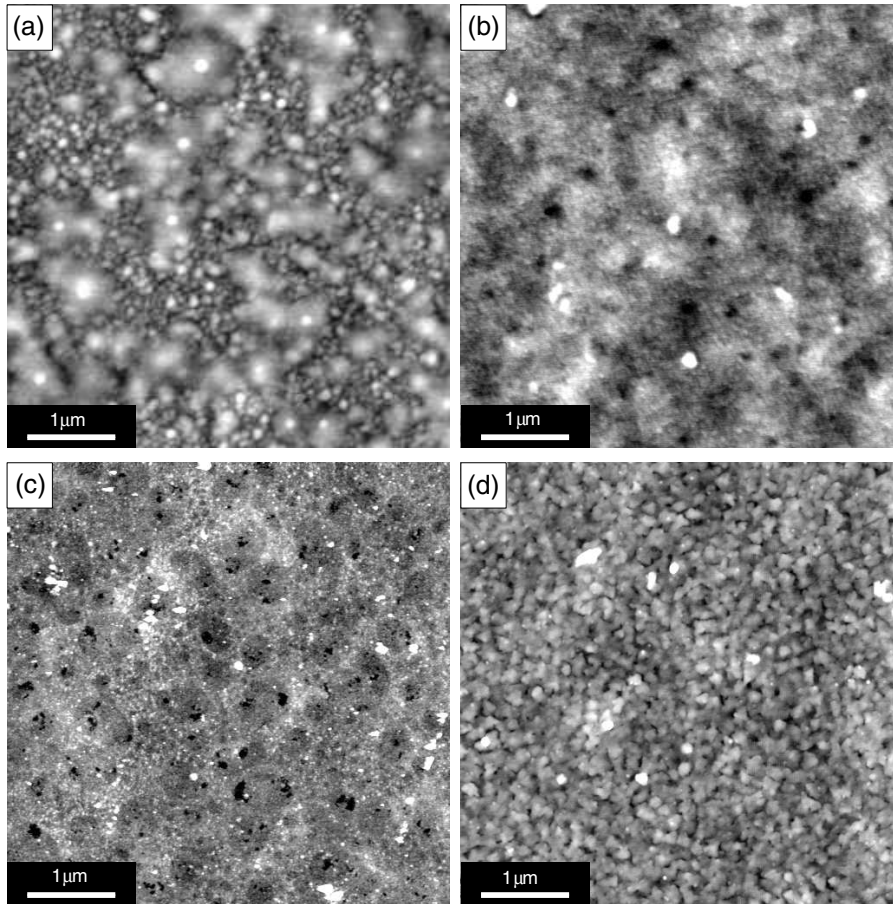


Figure 1. 5 μm AFM images of a typical MnSb film after sequential surface treatments ((a)–(c)) and an Sb-capped sample (d). An untreated, uncapped air-stored sample is shown in panel (a), for which the RMS roughness is 1.90 nm. After 30 s of ultrasonic treatment in acetone, the RMS roughness falls to 0.54 nm, panel (b), but increases to 1.85 nm after a 10 s etch in HCl and a rinse in deionized water, panel (c). A few sub-micron sized pits and mesas can be seen in (b) and (c) while the Sb-capped sample (d) has a more uniform morphology of connected Sb islands and a RMS roughness of 0.75 nm.

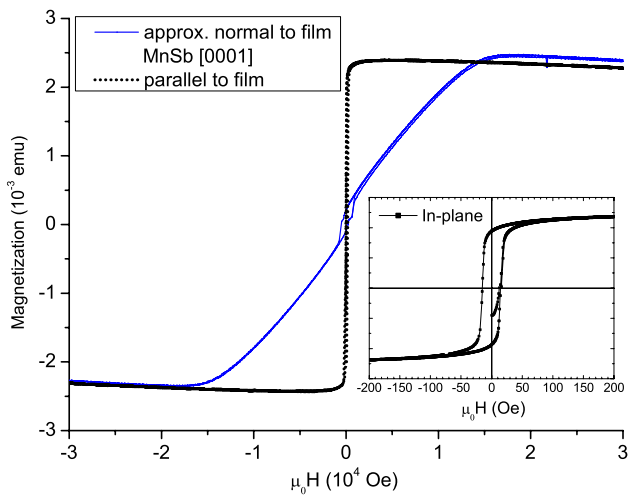


Figure 2. Hysteresis loops measured in-plane and out-of-plane by VSM for a 1 μm thick MnSb epilayer on GaAs(111)B.

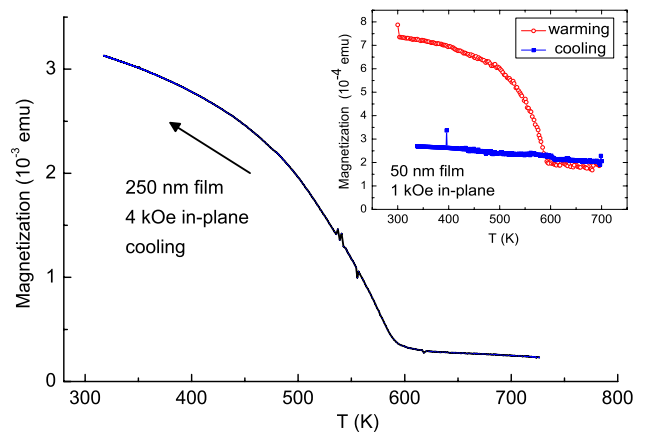


Figure 3. Temperature-dependent SQUID magnetometry results for two MnSb epilayers on GaAs(111)B. The main curve shows a 250 nm thick film being cooled from 730 K while the inset shows warming (\circ) and cooling (\blacksquare) of a thin (50 nm) epilayer.

Figure 2 shows room-temperature hysteresis loops from a 1 μm thick film (the main loops include a small diamagnetic contribution from the GaAs substrate). The inset shows

an in-plane hysteresis loop at low external field with substrate correction applied. The coercive field is 14.9 ± 0.5 Oe. The coercive fields are larger when aligned along

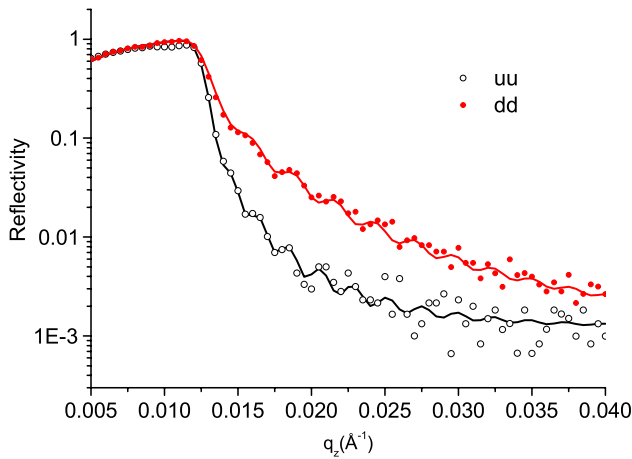


Figure 4. Polarized neutron reflectivity for a MnSb epilayer on GaAs(111). Experimental data are shown as circles (○ is the uu channel, ● is the dd channel) while the solid lines are fits generated using a simple three-layer model described in the text.

the perpendicular direction, MnSb [0001], while they are identical along the in-plane $[2\bar{1}\bar{1}0]$ and $[\bar{1}100]$ directions. This uniaxial anisotropy is in agreement with both first principles calculations [24] and the experimental magnetocrystalline anisotropy [25]. High quality epilayers more than ≈ 50 nm thick typically show in-plane coercivities below 20 Oe but we observe no correlation between film thickness and coercivity. Probably due to the high quality and uniformity of our films, these values of coercivity are significantly lower than those found by other groups for MnSb films grown on other substrates [26–28]. For example, Low *et al* [27] measured coercivities between 257 and 571 Oe for granular MnSb films grown by hot wall epitaxy on GaAs(001), which showed no out-of-plane hysteresis. The saturation field is much higher in the [0001] direction, typically 1.7×10^4 Oe compared to ~ 100 Oe in-plane.

The Curie temperatures of several films were measured in an external field (e.g. figure 3) and fell in the range $T_C = 589 \pm 5$ K with no discernible dependence on the field. However, after heating to high temperatures in the SQUID magnetometer, thinner MnSb films lost their magnetization permanently. An example is shown in the inset of figure 3, where a 50 nm thick film was heated to 700 K and then cooled. On cooling, the magnetization did not reappear. Although MnSb oxidizes readily [19], the background gas pressure in the SQUID is dominated by the He. Furthermore, scanning electron micrographs (not shown) indicate considerable disruption of the previously very flat films, which are too rough to image by AFM. We therefore attribute the loss of magnetization to the physical decomposition of the MnSb films at high temperature rather than to oxidation.

We now move on to depth-sensitive magnetic measurements. Typical PNR data are shown in figure 4 for a MnSb sample of thickness $235 \text{ nm} \pm 10 \text{ nm}$. The difference between the uu and dd curves shows the strong FM contribution to the PNR. Since the two reflectivity curves are coincident close to the critical angle ($q_z \approx 0.012 \text{ \AA}^{-1}$), a non-magnetic surface layer is clearly present. The data were fitted using the GenX

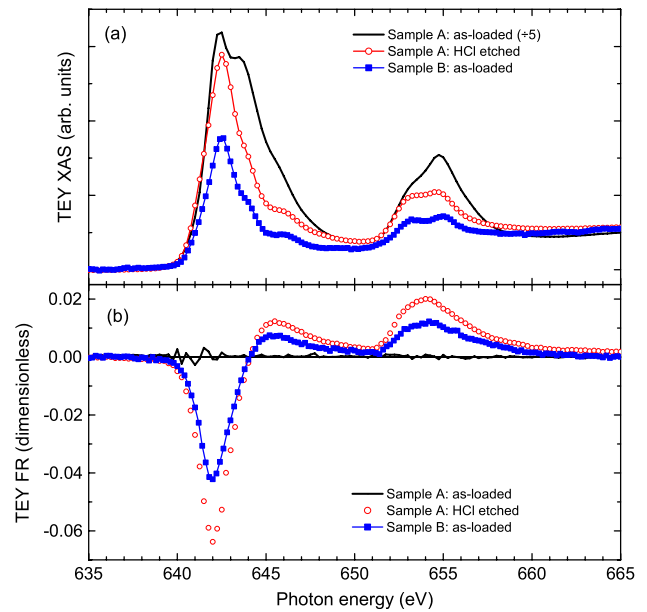


Figure 5. (a) Mn L-edge TEY XAS data for an uncapped sample (A) before (solid line) and after (○) a 40 s HCl etch, and for an Sb-capped sample denoted as B (■). The as-loaded TEY XAS intensity has been scaled down by a factor of 5. (b) XMCD measured by TEY FR for the same samples (same symbols, no scaling).

code [29] and the full structure could be described with just three layers. These were a semi-infinite GaAs substrate, an FM MnSb layer and a non-magnetic surface layer which was modelled as MnO [19]. The interface and surface roughness values for these layers were unconstrained, as was the thickness of the MnO surface layer ($7 \text{ nm} \pm 5 \text{ nm}$), while the total thickness of MnSb plus surface layer ($245 \text{ nm} \pm 7 \text{ nm}$) agreed with electron microscopy measurements ($235 \text{ nm} \pm 10 \text{ nm}$). The MnO layer had RMS surface roughness values of around 3 nm, although there was no measurable roughness at the GaAs–MnSb interface. The total spin moment of the MnSb was unconstrained and gave a value of $(3.5 \pm 0.15)\mu_B$, in agreement with previous determinations [30]. Our picture of the MnSb–GaAs(111) epilayers is therefore quite simple: a uniformly magnetized MnSb layer has a very sharp interface with the GaAs substrate and there is a rough, non-magnetic native oxide layer several nm thick. The MnSb epilayers were investigated further using x-ray measurements, where the vacuum sample environment allowed chemically etched surfaces to be measured without significant re-oxidation.

In figure 5(a) we show the Mn L-edge XAS measured by TEY before and after 40 s of HCl etching for an uncapped sample (A), as well as for an Sb-capped sample (B). The spectra were normalized to the photon flux, which was incident at 30° to the surface, and have then been scaled for clarity. The intensity for sample A before etch is about five times greater than that for sample A post-etch or for sample B. The reduction of normalized TEY intensity in sample A after etching is principally due to the increased RMS surface roughness from ≤ 1 nm to around 10 nm (cf figure 1—in general we found that longer acid etches produced rougher

MnSb surfaces). It is clear that the higher photon energy components of both the L_3 and L_2 edges of sample A are markedly reduced after the HCl etch. Due to the high surface specificity of the TEY measurement, this reduction of a higher energy component indicates the loss of surface-localized Mn bound to an element of higher electronegativity than Sb. We attribute this to the removal of the Mn-rich native oxides by the etch, which is consistent with our previous x-ray photoelectron spectroscopy (XPS) work [19]. Importantly, the TEY spectrum for Sb-capped sample B is very similar to that of the etched sample, indicating that the Sb cap has passivated the surface against the formation of Mn-rich native oxides.

In figure 5(b) the TEY flipping ratio (FR) at the Mn L-edge is shown for sample A before and after etching and for sample B. The FR is defined as being $[I_r - I_l]/[I_r + I_l]$ where I_r (I_l) is the signal from right (left) circularly polarized light. Very similar FR spectra are observed in XMCD and XRMS. It is clear that the untreated sample A shows no dichroism. Since the TEY measurement is highly surface-specific due to the short IMFP of the photoelectrons, this result is consistent with the presence of a non-FM film of Mn oxides at the surface. Using a value of 1.5 nm for the IMFP of a 650 eV photoelectron in MnO_2 [10] and assuming 95% attenuation in three IMFPs, the thickness of the oxide layer is estimated to be ≥ 4.5 nm, in good agreement with both our previous angle-dependent XPS determination of 4.6 nm [19] and the PNR results. After the etch a strong TEY dichroism signal is observed for sample A, indicating that FM behaviour is restored in the near-surface region due to removal of the oxide [19]. The TEY FR of the Sb-capped sample B strongly resembles that of the etched sample A indicating that the magnetic state of Mn atoms near the surface is identical in both cases, consistent with the removal of Mn oxides (A) or prevention of oxidation (B). The lower amplitude of the TEY FR for sample B (figure 5(b)) is caused by an increase in the sum term of the FR by photoemission of unpolarized electrons from the Sb capping layer. Both the XMCD and XAS Mn L-edge lineshapes resemble the calculated and experimental determinations of Kimura *et al* for a CuMn surface alloy [31]. The fine structures in our XAS spectra of sample A after etch and sample B are nearly identical and so are most unlikely to be due to residual oxide near the surface from two different surface passivation methods. Preliminary x-ray reflectivity experiments indicate Sb cap thicknesses of (4 ± 2) nm, but no detailed correlation of cap thickness and surface magnetic response in TEY has been attempted.

The integrated intensities of the $L_{2,3}$ edges can be related to the spin $\langle S_z \rangle$ and orbital $\langle L_z \rangle$ expectation values via sum rules, but application to early 3d transition metals such as Mn is known to be problematic [32, 33]. The sum rules demand that the $L_{2,3}$ edges are well separated such that the intensity of the TEY FR can be unambiguously assigned to each L-edge. However, the electrostatic interactions between ionized core levels and valence levels (2p–3d) are of similar magnitude to the spin–orbit coupling of the 2p states, causing *jj* mixing between the $2p_{1/2}$ and $2p_{3/2}$ channels [34–36]. Unambiguous assignment is difficult, although previous studies of elemental Mn on ferromagnetic substrates [35] indicate that the problem

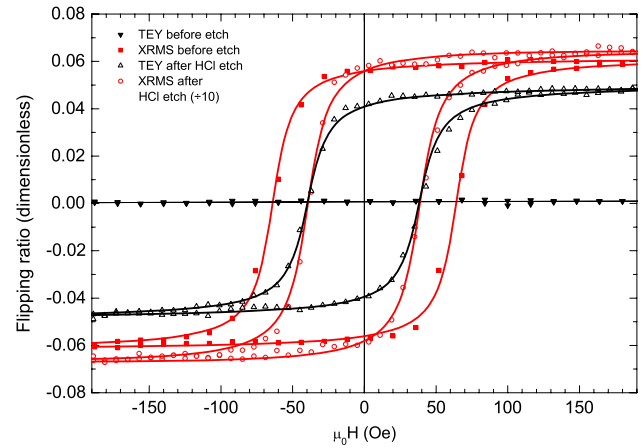


Figure 6. Hysteresis loops for an uncapped MnSb sample before and after etching based on TEY and XRMS FR (the solid lines are a guide to the eye).

can be overcome by multiplying the spin expectation value derived from the sum rules by 1.5. Using this approximate correction factor, the orbital-to-spin ratio $\langle L_z \rangle / \langle S_z \rangle$ for the Sb-capped MnSb samples was found to be 0.11 ± 0.01 . This is consistent with that found by Kimura [37] despite the different Mn environments. Recently, Krumme *et al* [38] studied Cu_2MnAl using XMCD, and using the correction factor for *jj* mixing found magnetic moments consistent with theory. However, there were persistent differences between the experimental and calculated Mn XMCD lineshapes apart from the integrated intensity ratio: in particular the calculated L_2 edge position is at too low an energy by 1–2 eV and the nonzero intensity between the main peaks is poorly reproduced, even in sign. Interestingly, our own preliminary density functional theory (DFT) calculations of XMCD for MnSb, using the same code as Krumme, show very similar discrepancies compared to the experiment. Krumme *et al* suggested that electronic correlations could be responsible for the spectral changes [38], which is also possible for MnSb. In the present case we can rule out surface effects as a source of the spectral features due to the high similarity of the XMCD and XRMS dichroism.

Hysteresis loops derived from both TEY and XRMS are shown in figure 6 for sample A. The FR was measured at a photon energy just below the Mn L_3 resonance, as a function of applied magnetic field at RT. No magnetic signal is observed in the TEY FR for the untreated oxidized sample, as expected from the results shown in figure 5(b). However, the oxidized sample shows clear hysteresis in the XRMS with a coercivity of 65 Oe. Due to the lower surface specificity of the XRMS signal the FM response of the underlying MnSb layer is still observed. After etching the coercive field is reduced to 40 Oe and the magnitude of the XRMS FR at saturation increases. The latter change arises since the difference term of the FR remains similar due to the FM MnSb but the sum term no longer includes the contribution from the non-magnetic oxide layer. The TEY FR also shows hysteresis with the same coercive field of 40 Oe after etching. The similar shape and coercivity of the XRMS and TEY loops

indicate a rather uniform magnetic response through the film: residual contamination, non-stoichiometry or roughness are not affecting the near-surface magnetic behaviour.

Competition between FM and anti-FM exchange interactions has previously been inferred from SPLEEM for Fe–NiO multi-layers [39] and similar interfacial exchange interactions between MnSb and Mn oxides, such as locally randomized exchange bias, are likely to cause the increased coercive field in the oxidized films. While NiO is widely used for RT exchange bias in magnetic multi-layers, stoichiometric Mn oxides are paramagnetic at RT. Anti-FM behaviour has been observed above the bulk Néel temperature in defective MnO [40] and such effects may occur in the non-stoichiometric ultra-thin film native oxides present in these samples. After the HCl etch, Mn does not re-oxidize to sufficient thickness to support interfacial exchange interactions and so the coercivity of the unbiased MnSb film is observed. These results suggest the possibility of deliberately tuning the properties of Mn pnictide films by controlled oxidation in a magnetic field.

The samples for SPLEEM showed a diffuse MnSb(0001)-(1 × 1) LEED pattern after etching, degassing and Ar sputtering. After raising the temperature to 675 K, the LEED pattern showed a sharp (2 × 2) symmetry as expected for MnSb(0001) [6]. However, the samples initially showed no magnetic domain contrast, possibly indicating the presence of a single FM domain much larger than the microscope's field-of-view. After annealing to 520 K and AC demagnetization, magnetic domains were observed and a typical SPLEEM image is shown in figure 7. The contrast (vertical scale bar) is an FR analogous to the x-ray measurements, i.e. the normalized intensity difference between consecutive LEEM images with opposite in-plane SP. Magnetic domains are clearly visible in figure 7 as broad light and dark features on the image. The highest magnetic contrast was observed at an electron energy of 6.0 ± 0.2 eV with respect to the Fermi energy. Systematic changes of the SP vector indicated that the magnetization of the domains was purely in-plane. The surface specificity of the SPLEEM measurement is even higher than that of the TEY XMCD since the IMFP for electrons of a few eV energy is extremely short, and the SPLEEM data clearly indicate that the ferromagnetism of the MnSb film persists to the surface.

In figure 8 are shown four LEEM images of MnSb during annealing to increasing temperatures in UHV. Contrast arises due to local chemical inhomogeneities at the surface as well as from interference effects due to the surface topography. The surface does not change significantly in the annealing temperature range 520–580 K. At higher temperatures, dark features appear in the images, which we interpret as local thermal decomposition of the MnSb film. Some of these features can be seen to grow during *in situ* imaging, such as the bottom left feature in panels (c) and (d) of figure 8. Extended annealing at a fixed temperature of 630 K also showed the growth of dark patches in the LEEM images. Annealing to 750 K resulted in more rapid changes of the surface morphology and complete degradation of the MnSb film structure. These UHV results are consistent with the complete loss of magnetization for thin epilayers after

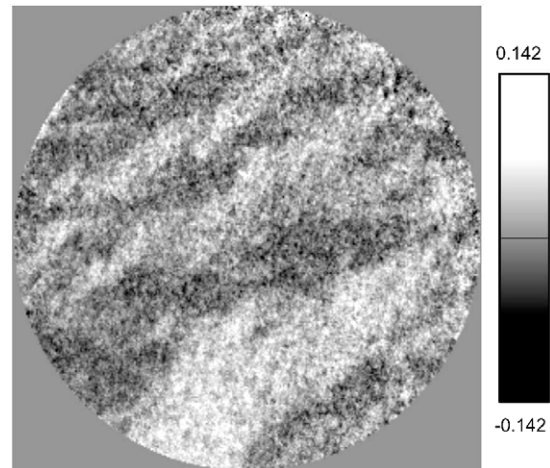


Figure 7. Contrast-optimized SPLEEM image of an uncapped, HCl-etched MnSb sample after UHV annealing to 520 K. The integration time was 5 s with an electron beam energy of 6.2 eV and the SP was in-plane. The field-of-view is $8 \mu\text{m}$ and the FR greyscale is explained in the text.

annealing to 700 K in the SQUID magnetometer (figure 3 inset). Further work is needed to clarify the thermal stability of the films under different conditions (UHV, inert gas, ambient, etc). Nonetheless, these results show that structurally ordered FM surfaces of etched MnSb films can be re-prepared in UHV; such surfaces would, for example, be suitable for epitaxial overgrowth of other materials or ordered molecular adsorption studies.

4. Conclusion

We have investigated the magnetism of MnSb(0001) thin films using PNR, XMCD, XRMS and SPLEEM. The differing surface specificities of the techniques provide a depth-dependent characterization of the thin film magnetism, in particular including the effects of the surface oxide. The native oxide of MnSb is Mn-rich, ~ 4.5 nm thick and can be removed by a simple HCl etch or prevented from forming by a thin Sb capping layer. The MnSb–GaAs and MnSb–oxide interfaces are sharp but longer HCl etches increase the surface roughness. The increased coercivity for oxidized MnSb films may be due to local interface exchange bias by the surface layer of Mn oxides. After HCl etching and gentle surface treatment in UHV, in-plane magnetized domains on MnSb(0001) were observed by SPLEEM. Although heating to ≥ 630 K begins to damage the film, ordered MnSb surfaces showing FM behaviour can be prepared in this way. Etched Mn pnictide films could be used as substrates for epitaxial overgrowth even after air exposure or processing, and could have their magnetic properties tuned by controlled oxidation. The total magnetic moment and orbital-to-spin ratio for Mn were found to be consistent with previous determinations. While the detailed spectral features associated with Mn XMCD remain difficult to interpret, as is the case for other Mn-containing alloys, we can rule out surface effects as a source of the fine structure.

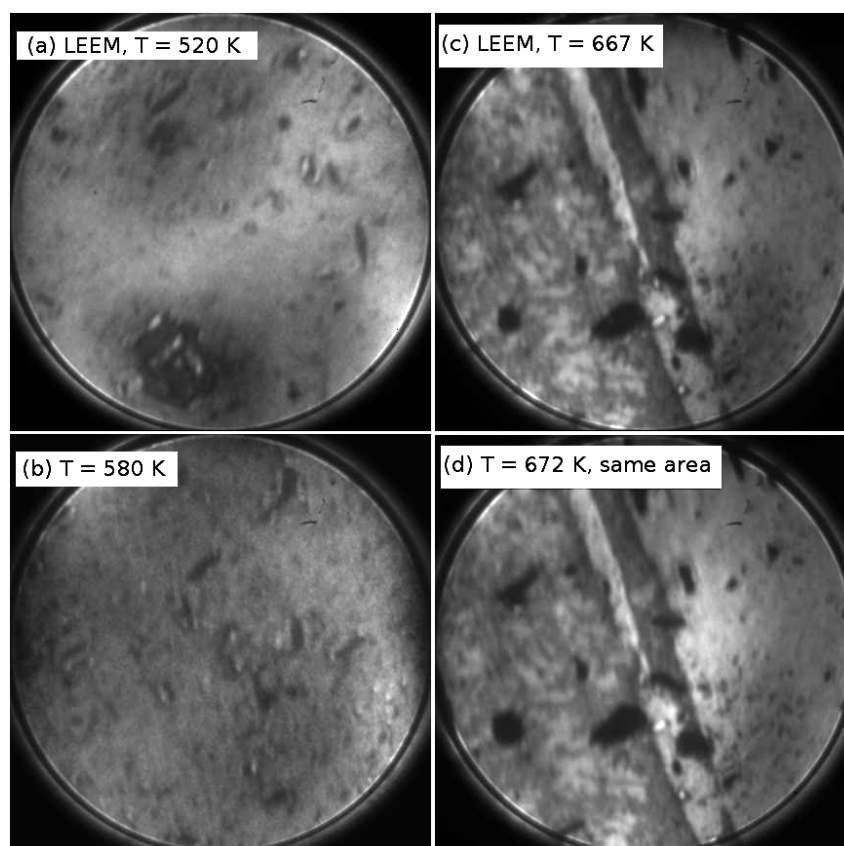


Figure 8. Typical LEEM images during annealing in UHV. The field-of-view is $8 \mu\text{m}$ and images (c) and (d) are taken sequentially from the same region of the sample. .

Acknowledgments

The authors are grateful for the technical expertise of R Johnston and S York. D Paul, M Wolff and K Zhernenkov provided invaluable assistance and advice with the neutron experiments. This work was supported by EPSRC (UK) via research studentships and grant EP/H041222/1. The US Department of Energy supported both the experiments at NSLS (Brookhaven National Laboratory) and the SPLEEM work, under contract numbers DE-AC02-98CH10886 and DEAC02-05CH11231 respectively.

References

- [1] Hai P H, Ohya S, Tanaka M, Barnes S E and Maekawa S 2009 *Nature* **458** 489
- [2] Awschalom D D and Flatté M E 2007 *Nature Phys.* **3** 153
- [3] Amemiya T, Ogawa Y, Shimizu H, Munekata H and Nakano Y 2008 *Appl. Phys. Express* **1** 022002
- [4] Shimizu H, Goto S and Mori T 2010 *Appl. Phys. Express* **3** 072201
- [5] Gregg J F 2007 *Nature Mater.* **6** 798
- [6] Hatfield S A and Bell G R 2007 *Surf. Sci.* **61** 5368
- [7] Varalda J, de Oliveira A J A, Ouerghi A, Eddrief M, Marangolo M, Demaille D, Etgens V H, Mattoso N and Mosca D H 2006 *J. Appl. Phys.* **100** 093524
- [8] Kurahashi M, Sun X and Yamauchi Y 2010 *Phys. Rev. B* **81** 193402
- [9] Yu H L and Yang G W 2011 *Appl. Phys. Lett.* **98** 011910
- [10] NIST Electron IMFP Database accessed September 2010 www.nist.gov/srd/nist71.htm
- [11] de Groot R A, Mueller F M, van Engen P G and Buschow K H 1983 *Phys. Rev. Lett.* **50** 2024
- [12] Galanakis I and Mavropoulos Ph 2003 *Phys. Rev. B* **67** 104417
- [13] Li S, Duh J-G, Bao F, Liu K-X, Kuo C-L, Wu X, Lü L, Huang Z and Du Y 2008 *J. Phys. D: Appl. Phys.* **41** 175004
- [14] Wang F, Fukuhara T, Maezawa K, Nishimura K, Shimizu F and Masubuchi S 2010 *Japan. J. Appl. Phys.* **49** 025502
- [15] Jenkins S J 2004 *Phys. Rev. B* **70** 245401
- [16] de Wijs G A and de Groot R A 2001 *Phys. Rev. B* **64** 020402(R)
- [17] Sicota M, Turban P, Andrieu S, Tagliaferri A, De Nadai C, Brookes N B, Bertran F and Fortuna F 2006 *J. Magn. Mater.* **303** 54
- [18] Correa J S, Eibl Ch, Rangelov G, Braun J and Donath M 2006 *Phys. Rev. B* **73** 125316
- [19] Hatfield S A, Aldous J D and Bell G R 2009 *Appl. Surf. Sci.* **225** 3567–75
- [20] Eickhoff Ch, Kolev H, Donath M, Rangelov G and Chi L F 2007 *Phys. Rev. B* **76** 205440
- [21] Kolev H, Rangelov G, Braun J and Donath M 2005 *Phys. Rev. B* **72** 104415
- [22] Sánchez-Hanke C, Kao C-C and Hulbert S L 2009 *Nucl. Instrum. Methods A* **608** 351–9
- [23] Grzelakowski K, Duden T, Bauer E, Poppa H and Chiang S 1994 *IEEE Trans. Magn.* **30** 4500
- [24] Vast N, Siberchicot B and Zerah P G 1992 *J. Phys.: Condens. Matter* **4** 10469
- [25] Okita T and Makino Y 1968 *J. Phys. Soc. Japan* **25** 120
- [26] Zhang H, Kushvaha S S, Wee A T S and Wang X-S 2007 *J. Appl. Phys.* **102** 023906

- [27] Low B L, Ong C K, Han G C, Gong H, Liew T Y F, Tatsuoka H, Kuwabara H and Yang Z 1998 *J. Appl. Phys.* **84** 973
- [28] Tatsuoka H, Isaji K, Kuwabara H, Nakanishi Y, Nakamura T and Fujiyasu H 1997 *Appl. Surf. Sci.* **113** 48
- [29] Björk M and Andersson G 2007 *J. Appl. Crystallogr.* **40** 1174
- [30] Coehoorn R, Haas C and de Groot R A 1985 *Phys. Rev. B* **31** 1980–96
- [31] Kimura A, Kanbe T, Xie T, Qiao S, Taniguchi M, Muro T, Imada S and Suga S 2003 *Japan. J. Appl. Phys.* **42** 4692
- [32] Thole B T, Carra P, Sette F and van der Laan G 1992 *Phys. Rev. Lett.* **68** 1943
- [33] Carra P, Thole B T, Altarelli M and Wang X 1993 *Phys. Rev. Lett.* **70** 694
- [34] Abes M *et al* 2010 *Phys. Rev. B* **82** 184412
- [35] Dürr H A, van der Laan G, Spanke D, Hillebrecht F U and Brookes N B 1997 *Phys. Rev. B* **56** 8156
- [36] O'Brien W L, Tonner B P, Harp G R and Parkin S S P 1994 *J. Appl. Phys.* **76** 6462
- [37] Kimura A, Suga S, Shishidou T, Imada S, Muro T, Park S Y, Miyahara T, Kaneko T and Kanomata T 1997 *Phys. Rev. B* **56** 6021–30
- [38] Krumme B, Herper H C, Erb D, Weis C, Antoniak C, Warland A, Westerholt K, Entel P and Wende H 2011 *J. Phys. D: Appl. Phys.* **44** 415004
- [39] Rougemaille N, Portalupi M, Brambilla A, Biagioni P, Lanzara A, Finazzi M, Schmid A K and Duò L 2007 *Phys. Rev. B* **76** 214425
- [40] Barber D J and Evans R G 1971 *J. Mater. Sci.* **6** 1237